Proceeding Series of the Brazilian Society of Computational and Applied Mathematics, v. 11, n. 1, 2025.

Trabalho apresentado no XLIII CNMAC, Centro de Convenções do Armação Resort - Porto de Galinhas - PE, 2024

Proceeding Series of the Brazilian Society of Computational and Applied Mathematics

A Mixed Finite Element Method for a $\mu(I)$-rheology Model of Granular Materials

Sergio Caucao[1]
DMFA/UCSC, Concepción, CL
Gabriel N. Gatica[2]
DIM/USC, Concepción, CL
Saulo R. Medrado[3], Yuri D. Sobral[4]
PPGMAT/UnB, Brasília, DF, BR

Abstract. We propose and analyze new mixed finite element methods for a regularized $\mu(I)$-rheology model of granular flows with an equivalent viscosity depending nonlinearly on the pressure and on the Euclidean norm of the symmetric part of the velocity gradient. To this end, and besides the velocity, the pressure and the aforementioned strain rate, we introduce a modified stress tensor that includes the convective term, and the skew-symmetric vorticity, as auxiliary tensor unknowns, thus yielding a mixed variational formulation within a Banach spaces framework. Then, the pressure is obtained through an iterative postprocess suggested by the incompressibility condition of the fluid, which allows us to express this unknown in terms of the aforementioned stress and the velocity. A fixed-point strategy combined with a solvability result for a class of nonlinear twofold saddle point operator equations in Banach spaces, are employed to show, along with the classical Banach fixed-point theorem, the well-posedness of the continuous and discrete formulations. Optimal a priori error estimates are derived and associated rates of convergence are established. Finally, numerical results confirming the latter and illustrating the good performance of the method, are reported.

keywords. granular flows, nonlinear viscosity, twofold saddle point, mixed finite elements, fixed-point theory, a priori error analysis

1 Introduction

Granular flows are present in our daily lives in different scales: dust on the streets, pills in flasks or in pharmaceutical production lines and sand, that can be found in beaches and as dunes in deserts, for example.

One of the first attempts to use equations similar to the Navier-Stokes equations for granular flows was carried out in [11]. It was proposed in [10] that the dissipative nature of granular flows was due to frictional behavior, and that the frictional coefficient μ of the flow was governed by the dimensionless *inertial number* I, that compares the shear and collisional time scales in dense granular flows.

The major difficulty imposed by the $\mu(I)$-rheology model is the dependence of the dissipative terms on the pressure of the flow. In other words, the strong non-linearity of the $\mu(I)$-rheology model prevents us from guaranteeing in advance successful applications of classical numerical methods, such as primal finite elements and related techniques, which are known to be usually more

[1]scaucao@ucsc.cl
[2]ggatica@ci2ma.udec.cl
[3]saulo.medrado@aluno.unb.br
[4]ydsobral@unb.br

suitable for linear problems, particularly if they are posed within a Hilbertian framework. In this regard, we find it important to stress that the suitability of Banach spaces-based approaches to analyze the continuous and discrete solvabilities of diverse nonlinear problems in continuum mechanics, including several coupled models, and employing mainly mixed formulations, has been confirmed by a significant amount of contributions in recent years [3, 5–7].

Furthermore, one of the main advantages of employing a Banach framework is the fact that no augmentation is required, a common "trick" of Hilbert spaces-based formulations to force them to become, for instance, elliptic or strongly monotone, and hence the spaces to which the unknowns belong are the natural ones arising simply from the testing of the equations of the model along with the use of the Cauchy-Schwarz and Hölder inequalities. In this way, simpler and closer to the original physical model formulations are derived. In turn, the main benefits of employing a mixed approach include the derivation of momentum-conservative numerical schemes, and the possibility of obtaining direct approximations of further variables of physical interest, either by incorporating them into the formulation, or by employing a postprocessing formula in terms of the remaining unknowns.

According to the previous discussion, the goal of the present work is to introduce and analyze mixed finite element methods for numerically solving the steady-state $\mu(I)$-rheology equations for granular flows, as published in [4].

2 The Mathematical Model

We consider the flow of particles of constant density ρ_p and diameter d in Ω, denote by $\mathbf{u}$ the velocity of the flow, and assume that the latter is incompressible, so that the overall density is $\rho = \phi\rho_p$. The governing equations are given by:

$$\rho\left(\frac{\partial \mathbf{u}}{\partial t} + (\nabla \mathbf{u})\mathbf{u}\right) = \mathbf{div}(\boldsymbol{\sigma}) + \rho\,\mathbf{g} \quad \text{in} \quad \Omega\,, \quad \text{and} \quad \mathrm{div}(\mathbf{u}) = 0 \quad \text{in} \quad \Omega\,. \tag{1}$$

The stress tensor $\boldsymbol{\sigma}$ is composed of two terms, a deviatoric one associated to dissipation due to the internal friction of the medium, which is inspired by a Coulomb friction-like law, and an isotropic one related to the pressure p on the medium. More precisely, there holds

$$\boldsymbol{\sigma} = \sqrt{2}\,\mu\,p\,\frac{\mathbf{D}}{|\mathbf{D}|} - p\,\mathbb{I} \quad \text{in} \quad \Omega\,, \quad \mathbf{D} := \frac{1}{2}\Big(\nabla \mathbf{u} + (\nabla \mathbf{u})^{\mathrm{t}}\Big), \quad |\mathbf{D}| = \sqrt{\mathbf{D} : \mathbf{D}}\,. \tag{2}$$

where μ is the internal friction coefficient of the granular continuum, and $\mathbf{D}$ is the symmetric part of the velocity gradient. Thanks to the incompressibility condition, there holds $\mathrm{tr}(\mathbf{D}) = \mathrm{div}(\mathbf{u}) = 0$.

The flows of granular materials based on the $\mu(I)$-rheology approach introduced in [10] arose from the fundamental hypothesis that the corresponding stresses can be described by a visco-plastic constitutive equation in which the internal friction μ of the material, which governs the yield stress, depends on the local properties of the flow through the inertial number I, in the form

$$\mu(I) := \mu_s + \left(\frac{\mu_d - \mu_s}{I + I_0}\right) I \qquad \text{with} \qquad I = \frac{\sqrt{2}\,d\,|\mathbf{D}|}{\sqrt{p/\rho}}\,, \tag{3}$$

where the coefficients μ_s and μ_d correspond, respectively, to the static and dynamic friction limits, and I_0 is a reference (experimental) constant. Then, substituting (3) in the constitutive relation (2), we arrive at

$$\boldsymbol{\sigma} = \eta(p, |\mathbf{D}|)\,\mathbf{D} - p\,\mathbb{I} \quad \text{in} \quad \Omega\,, \tag{4}$$

where

$$\eta(\varrho, \omega) := \frac{a_1\,\varrho}{\omega + \varepsilon} + \frac{a_2\,\varrho}{a_3\,\sqrt{\varrho} + a_4\,\omega + \varepsilon} \qquad \forall\,(\varrho, \omega) \in \mathrm{R}^+ \times \mathrm{R}^+\,. \tag{5}$$

with $0 < \varepsilon \ll 1$ being a regularization parameter and positive coefficients a_i, $i \in \{1, 2, 3, 4\}$, given by $a_1 := \sqrt{2}\,\mu_s$, $a_2 := 2\,d(\mu_d - \mu_s)$, $a_3 := \rho^{-1/2}\,I_0$, and $a_4 := \sqrt{2}\,d$. Regarding boundary

conditions, and knowing that recent evidence [8] suggests that there can be some slip between the grains and the boundaries, we proceed accordingly and assume this condition for the steady-state regime that we consider. Then the governing equations of the stationary model are given by

$$\rho(\nabla\mathbf{u})\mathbf{u} = \mathbf{div}\big(\eta(p,|\mathbf{D}|)\,\mathbf{D}\big) - \nabla p + \rho\,\mathbf{g} \quad \text{in} \quad \Omega, \quad \mathrm{div}(\mathbf{u}) = 0 \quad \text{in} \quad \Omega, \quad \mathbf{u} = \mathbf{u}_D \quad \text{on} \quad \Gamma\,, \tag{6}$$

In order to propose a fully-mixed finite element method for (6), we now introduce a modified stress tensor, still denoted $\boldsymbol{\sigma}$, as the further unknown defined by

$$\boldsymbol{\sigma} \,:=\, \eta(p,|\mathbf{D}|)\,\mathbf{D} \,-\, p\,\mathbb{I} \,-\, \rho\,(\mathbf{u}\otimes\mathbf{u})\,. \tag{7}$$

Remembering that that

$$\boldsymbol{\gamma} \,:=\, \frac{1}{2}\,\Big(\nabla\mathbf{u} \,-\, (\nabla\mathbf{u})^{\mathtt{t}}\Big)\,, \tag{8}$$

we can reformulate (6) as the equivalently problem: Find $\mathbf{D}$, $\boldsymbol{\sigma}$, $\mathbf{u}$, p, and $\boldsymbol{\gamma}$ in suitable spaces, to be defined later on, such that

$$\begin{gathered}\mathbf{D} \,-\, \nabla\mathbf{u} \,+\, \boldsymbol{\gamma} = 0 \quad \text{in} \quad \Omega\,, \quad \eta(p,|\mathbf{D}|)\,\mathbf{D} \,-\, \boldsymbol{\sigma}^{\mathtt{d}} \,-\, \rho\,(\mathbf{u}\otimes\mathbf{u})^{\mathtt{d}} = 0 \quad \text{in} \quad \Omega\,,\\ \mathbf{div}(\boldsymbol{\sigma}) \,+\, \mathbf{f} = 0 \quad \text{in} \quad \Omega\,, \quad p \,=\, -\frac{1}{n}\,\mathrm{tr}\big(\boldsymbol{\sigma} \,+\, \rho\,(\mathbf{u}\otimes\mathbf{u})\big) \quad \text{in} \quad \Omega\,, \quad \mathbf{u} = \mathbf{u}_D \quad \text{on} \quad \Gamma\,.\end{gathered} \tag{9}$$

3 The Continuous Formulation

Multiplying the equations in (9) by test functions from appropriate Banach function spaces, we derive the following mixed variational formulation: Given $p \in \mathrm{L}^2(\Omega)$, find $(\mathbf{D},\boldsymbol{\sigma},\mathbf{u},\boldsymbol{\gamma}) \in \mathcal{H}_1 \times \mathcal{H}_2 \times \mathcal{Q}_1 \times \mathcal{Q}_2$ such that

$$\begin{aligned}\int_\Omega \eta(p,|\mathbf{D}|)\,\mathbf{D}:\mathbf{E} \qquad - \int_\Omega \boldsymbol{\sigma}:\mathbf{E} \qquad\qquad - \rho\int_\Omega (\mathbf{u}\otimes\mathbf{u}):\mathbf{E} \qquad &= \quad 0\,,\\ -\int_\Omega \boldsymbol{\tau}:\mathbf{D} \qquad\qquad\qquad\qquad - \int_\Omega \mathbf{u}\cdot\mathbf{div}(\boldsymbol{\tau}) - \int_\Omega \boldsymbol{\tau}:\boldsymbol{\gamma} \quad &= \quad -\langle\boldsymbol{\tau}\,\boldsymbol{\nu},\mathbf{u}_D\rangle\,,\\ - \int_\Omega \mathbf{v}\cdot\mathbf{div}(\boldsymbol{\sigma}) - \int_\Omega \boldsymbol{\sigma}:\boldsymbol{\xi} \qquad\qquad\qquad\qquad &= \quad \int_\Omega \mathbf{f}\cdot\mathbf{v}\,,\end{aligned} \tag{10}$$

for all $(\mathbf{E},\boldsymbol{\tau},\mathbf{v},\boldsymbol{\xi}) \in \mathcal{H}_1 \times \mathcal{H}_2 \times \mathcal{Q}_1 \times \mathcal{Q}_2$.

We employ a fixed-point approach along with an abstract result on the well-posedness of the aforementioned type of nonlinear operator equations in Banach spaces, to analyze the solvability of the mixed variational formulation (10), introducing the operator $\mathbf{T} : \mathcal{Q}_1 \times \mathrm{L}^2_\kappa(\Omega) \longrightarrow \mathcal{Q}_1 \times L^2_\kappa(\Omega)$ defined as

$$\mathbf{T}(\mathbf{z},r) \,:=\, (\mathbf{u},p) \qquad \forall\,(\mathbf{z},r) \,\in\, \mathcal{Q}_1 \times \mathrm{L}^2_\kappa(\Omega)\,, \tag{11}$$

where $(\mathbf{D},\boldsymbol{\sigma},\vec{\mathbf{u}}) \,:=\, \big(\mathbf{D},\boldsymbol{\sigma},(\mathbf{u},\boldsymbol{\gamma})\big) \in \mathcal{H}_1 \times \mathcal{H}_2 \times \mathcal{Q}$ is the unique solution of the problem arising from (10) replacing p with r, and one of $\mathbf{u}$ with $\mathbf{z}$ in the nonlinear term involving $\mathbf{u}$, and p is computed as

$$p \,:=\, -\frac{1}{n}\,\mathrm{tr}\big(\boldsymbol{\sigma} + \rho\,(\mathbf{u}\otimes\mathbf{u})\big) \,+\, \frac{\kappa}{|\Omega|} \,+\, \frac{\rho}{n\,|\Omega|}\int_\Omega \mathrm{tr}(\mathbf{u}\otimes\mathbf{u})\,. \tag{12}$$

Then, it is readily seen that solving (10) is equivalent to finding a fixed point of $\mathbf{T}$, that is $(\mathbf{u},p) \in \mathcal{Q}_1 \times \mathrm{L}^2_\kappa(\Omega)$ such that

$$\mathbf{T}(\mathbf{u},p) \;=\; (\mathbf{u},p)\,. \tag{13}$$

We prove that the operator $\mathbf{T}$ in Eq.(11) is well-defined, for which we make use of an abstract result establishing sufficient conditions for the well-posedness of a class of twofold saddle point operator equations. The details are avaliable in [4]. Knowing that $\mathbf{T}$ is well-defined, we now address the solvability of the fixed-point equation (13). We begin the analysis deriving sufficient conditions on $\mathbf{T}$ to map a complete metric subspace of $\mathcal{Q}_1 \times \mathrm{L}^2_\kappa(\Omega)$ into itself.

4 The Galerkin Scheme

We introduce the Galerkin scheme for the fully-mixed variational formulation (10), analyze its solvability using a discrete version of the fixed-point approach as employed in Section 3, and derive the corresponding a priori error estimate.

We begin by letting $\mathcal{H}_{1,h}$, $\mathcal{H}_{2,h}$, $\mathcal{Q}_{1,h}$, and $\mathcal{Q}_{2,h}$ be arbitrary finite dimensional subspaces of $\mathcal{H}_1$, $\mathcal{H}_2$, $\mathcal{Q}_1$, and $\mathcal{Q}_2$, respectively, and let $\mathcal{P}_h := \widetilde{\mathcal{P}}_h \oplus \left\{\frac{\kappa}{|\Omega|}\right\}$, where $\widetilde{\mathcal{P}}_h$ is a finite dimensional subspace of $\mathrm{L}^2_0(\Omega) := \left\{q \in \mathrm{L}^2(\Omega) : \quad \int_\Omega q \,=\, 0\right\}$. If these subspaces satisfy specific hypotheses, we can prove the solvability of the discrete problem, and derive the Céa estimate for the Galerkin error given by

$$\|\vec{\mathbf{D}} - \vec{\mathbf{D}}_h\|_{\mathcal{H}} + \|p - p_h\|_{0,\Omega} := \|\mathbf{D} - \mathbf{D}_h\|_{0,\Omega} + \|\boldsymbol{\sigma} - \boldsymbol{\sigma}_h\|_{\mathbf{div}_{4/3};\Omega} + \|\vec{\mathbf{u}} - \vec{\mathbf{u}}_h\|_{\mathcal{Q}} + \|p - p_h\|_{0,\Omega}\,,$$

where $\vec{\mathbf{D}} := (\mathbf{D}, \boldsymbol{\sigma}, \vec{\mathbf{u}}) = \big(\mathbf{D}, \boldsymbol{\sigma}, (\mathbf{u}, \boldsymbol{\gamma})\big) \in \mathcal{H} := \mathcal{H}_1 \times \mathcal{H}_2 \times \mathcal{Q}$ is the unique solution of (10), with, and $\vec{\mathbf{D}}_h := (\mathbf{D}_h, \boldsymbol{\sigma}_h, \vec{\mathbf{u}}_h) = \big(\mathbf{D}_h, \boldsymbol{\sigma}_h, (\mathbf{u}_h, \boldsymbol{\gamma}_h)\big) \in \mathcal{H}_h := \mathcal{H}_{1,h} \times \mathcal{H}_{2,h} \times \mathcal{Q}_{1,h} \times \mathcal{Q}_{2,h}$ is the unique solution of discrete version of (10), whereas p and p_h are computed according to (12) and (12).

We are now in position to establish the main result of this section, that is, we can prove that, with some conditions, there exists a positive constant C, independent of h, such that

$$\|\vec{\mathbf{D}} - \vec{\mathbf{D}}_h\|_{\mathcal{H}} + \|p - p_h\|_{0,\Omega} \,\leq\, C\,\mathrm{dist}(\vec{\mathbf{D}}, \mathcal{H}_h)\,. \tag{14}$$

5 Specific Finite Element Subspaces

We make use of the regular family of triangulations $\{\mathcal{T}_h\}_{h>0}$ of $\overline{\Omega}$. Given an integer $\ell \geq 0$ and $K \in \mathcal{T}_h$, we let $\mathrm{P}_\ell(K)$ be the space of polynomials of degree $\leq \ell$ defined on K, and denote its vector and tensor versions by $\mathbf{P}_\ell(K) := [\mathrm{P}_\ell(K)]^n$ and $\mathbb{P}_\ell(K) = [\mathrm{P}_\ell(K)]^{n\times n}$, respectively. In addition, we let $\mathbb{RT}_\ell(K) := \mathbf{P}_\ell(K) \oplus \mathrm{P}_\ell(K)\,\mathbf{x}$ be the local Raviart–Thomas space of order ℓ defined on K, where $\mathbf{x}$ stands for a generic vector in $\mathbf{R} := \mathrm{R}^n$. Also, we let b_K be the bubble function on K, which is defined as the product of its $n+1$ barycentric coordinates. Then, we define the local bubble spaces of order ℓ as

$$\mathbf{B}_\ell(K) := \mathrm{curl}\,\big(b_K\,\mathrm{P}_\ell(K)\big) \quad \text{if} \quad n = 2\,, \quad \text{and} \quad \mathbf{B}_\ell(K) := \mathrm{curl}\,\big(b_K\,\mathbf{P}_\ell(K)\big) \quad \text{if} \quad n = 3\,, \tag{15}$$

where $\mathrm{curl}\,(v) := \big(\frac{\partial v}{\partial x_2}, -\frac{\partial v}{\partial x_1}\big)$ if $n = 2$ and $v : K \to \mathrm{R}$, and $\mathrm{curl}\,(\mathbf{v}) := \nabla \times \mathbf{v}$ if $n = 3$ and $\mathbf{v} : K \to \mathrm{R}^3$.

Using the global versions of polynomial spaces defined above, we can define two examples of finite-dimensional subspaces. One example is the Plane Elasticity Element with Reduced Symmetry (PEERS) of order $\ell \geq 0$, which, denoting $\mathbb{C}(\bar{\Omega}) := [C(\bar{\Omega})]^{n\times n}$, is given by

$$\mathcal{H}_{1,h} := \mathbb{P}_{\ell+n}(\Omega) \cap \mathcal{H}_1\,, \quad \widetilde{\mathcal{H}}_{2,h} := \mathbb{RT}_\ell(\Omega) \oplus \mathbb{B}_\ell(\Omega)\,, \quad \mathcal{Q}_{1,h} := \mathbf{P}_\ell(\Omega)\,, \quad \mathcal{Q}_{2,h} := \mathbb{C}(\bar{\Omega}) \cap \mathbb{P}_{\ell+1}(\Omega) \cap \mathcal{Q}_2\,, \tag{16}$$

and Arnold-Falk-Winther (AFW) element of order $\ell \geq 0$, (cf. [2]), given by

$$\mathcal{H}_{1,h} := \mathbb{P}_{\ell+1}(\Omega) \,\cap\, \mathcal{H}_1\,, \quad \widetilde{\mathcal{H}}_{2,h} := \mathbb{P}_{\ell+1}(\Omega) \cap \mathbb{H}(\mathbf{div};\Omega)\,, \quad \mathcal{Q}_{1,h} := \mathbf{P}_\ell(\Omega)\,, \quad \mathcal{Q}_{2,h} := \mathbb{P}_\ell(\Omega) \cap \mathcal{Q}_2\,. \tag{17}$$

Then, assuming that there exists $r \in (0, \ell+1]$, such that $\mathbf{D} \in \mathbb{H}^r(\Omega) \cap \mathbb{L}^2_{\mathrm{tr}}(\Omega)$, $\boldsymbol{\sigma} \in \mathbb{H}^r(\Omega) \cap \mathbb{H}_0(\mathbf{div}_{4/3};\Omega)$, $\mathbf{div}(\boldsymbol{\sigma}) \in \mathbf{W}^{r,4/3}(\Omega)$, $\mathbf{u} \in \mathbf{W}^{r,4}(\Omega)$, and $\boldsymbol{\gamma} \in \mathbb{H}^r(\Omega) \cap \mathcal{Q}_2$, we show that there exists a positive constant C, independent of h, such that:

$$\|\vec{\mathbf{D}} - \vec{\mathbf{D}}_h\|_{\mathcal{H}} + \|p - p_h\|_{0,\Omega} \,\leq\, C\,h^r \left\{\|\mathbf{D}\|_{r,\Omega} + \|\boldsymbol{\sigma}\|_{r,\Omega} + \|\mathbf{div}(\boldsymbol{\sigma})\|_{r,4/3;\Omega} + \|\mathbf{u}\|_{r,4;\Omega} + \|\boldsymbol{\gamma}\|_{r,\Omega}\right\}.$$

6 Numerical Results

We refer to the corresponding sets of finite element subspaces generated by $\ell = \{0, 1\}$ as simply PEERS_ℓ and AFW_ℓ based discretizations. The numerical methods have been implemented using the open source finite element library `FEniCS` [1]. We solve approximately the nonlinear problem (10) by means of a strategy combining a Picard iteration with the Newton method. More precisely, the corresponding computations are described as follows:

(1) Start solving the Stokes problem with constant viscosity arising from discrete version of (10) by choosing $\eta = 1$ and the overall density $\rho = 0$ to obtain the initial solution $(\mathbf{D}_h^0, \boldsymbol{\sigma}_h^0, \vec{\mathbf{u}}_h^0) := \big(\mathbf{D}_h^0, \boldsymbol{\sigma}_h^0, (\mathbf{u}_h^0, \boldsymbol{\gamma}_h^0)\big) \in \mathcal{H}_{1,h} \times \mathcal{H}_{2,h} \times \mathcal{Q}_h$, compute p_h^0 by

$$p_h^0 := -\frac{1}{n}\,\mathrm{tr}\big(\boldsymbol{\sigma}_h^0 + \rho\,(\mathbf{u}_h^0 \otimes \mathbf{u}_h^0)\big) + \frac{\kappa}{|\Omega|} + \frac{\rho}{n\,|\Omega|}\int_\Omega \mathrm{tr}(\mathbf{u}_h^0 \otimes \mathbf{u}_h^0)\,,$$

and let $m = 1$.

(2) Set $(\mathbf{z}_h, r_h) := (\mathbf{u}_h^{m-1}, p_h^{m-1})$ and let $(\mathbf{D}_h^m, \boldsymbol{\sigma}_h^m, \vec{\mathbf{u}}_h^m) := \big(\mathbf{D}_h^m, \boldsymbol{\sigma}_h^m, (\mathbf{u}_h^m, \boldsymbol{\gamma}_h^m)\big) \in \mathcal{H}_{1,h} \times \mathcal{H}_{2,h} \times \mathcal{Q}_h$ be the output of a single Newton iteration applied to discrete version of (11).

(3) Update the pressure p_h^m by employing the formula

$$p_h^m := -\frac{1}{n}\,\mathrm{tr}\big(\boldsymbol{\sigma}_h^m + \rho\,(\mathbf{u}_h^m \otimes \mathbf{u}_h^m)\big) + \frac{\kappa}{|\Omega|} + \frac{\rho}{n\,|\Omega|}\int_\Omega \mathrm{tr}(\mathbf{u}_h^m \otimes \mathbf{u}_h^m)\,,$$

let $m = m + 1$, and go to step (2).

The iterative procedure given by steps (2) and (3) is finished when the relative error between two consecutive iterations of the complete coefficient vector, namely $\mathbf{coeff}^m$ and $\mathbf{coeff}^{m+1}$, is sufficiently small, that is, $\|\mathbf{coeff}^{m+1} - \mathbf{coeff}^m\|_{\mathtt{DOF}}/\|\mathbf{coeff}^{m+1}\|_{\mathtt{DOF}} \leq \mathsf{tol}$, where $\|\cdot\|_{\mathtt{DOF}}$ stands for the usual Euclidean norm in $\mathrm{R}^{\mathtt{DOF}}$ with $\mathtt{DOF}$ denoting the total number of degrees of freedom defining the finite element subspaces $\mathcal{H}_{1,h}$, $\widetilde{\mathcal{H}}_{2,h}$, $\mathcal{Q}_{1,h}$, and $\mathcal{Q}_{2,h}$ (cf. (16)–(17)), and tol is a fixed tolerance chosen as $\mathsf{tol} = 1E-06$.

The individual errors are denoted by $\mathsf{e}(\mathbf{D}) := \|\mathbf{D} - \mathbf{D}_h\|_{0,\Omega}$, $\mathsf{e}(\boldsymbol{\sigma}) := \|\boldsymbol{\sigma} - \boldsymbol{\sigma}_h\|_{\mathbf{div}_{4/3};\Omega}$, $\mathsf{e}(\mathbf{u}) := \|\mathbf{u} - \mathbf{u}_h\|_{0,4;\Omega}$, $\mathsf{e}(\boldsymbol{\gamma}) := \|\boldsymbol{\gamma} - \boldsymbol{\gamma}_h\|_{0,\Omega}$, $\mathsf{e}(p) := \|p - p_h\|_{0,\Omega}$, and, as usual, for each $\star \in \big\{\mathbf{D}, \boldsymbol{\sigma}, \mathbf{u}, \boldsymbol{\gamma}, p\big\}$ we let $\mathsf{r}(\star)$ be the experimental rate of convergence given by $\mathsf{r}(\star) := \log(\mathsf{e}(\star)/\widehat{\mathsf{e}}(\star))/\log(h/\widehat{h})$, where h and $\widehat{h}$ denote two consecutive meshsizes with errors e and $\widehat{\mathsf{e}}$, respectively.

Example 1: Convergence Against Smooth Exact Solutions in a 2D Domain

In this test we corroborate the rates of convergence in a two-dimensional domain set by the square $\Omega = (0,1)^2$. We choose the regularization factor $\varepsilon = 1E-08$, and adjust the datum $\mathbf{f}$ in (9) such that the exact solution is given by

$$\mathbf{u}(x_1, x_2) = \begin{pmatrix} \sin(x_1)\cos(x_2) \\ -\cos(x_1)\sin(x_2) \end{pmatrix} \quad \text{and} \quad p(x_1, x_2) = \exp(x_1 + x_2), \tag{18}$$

where $p \in \mathrm{L}^2_\kappa(\Omega)$, with $\kappa = (\exp(1) - 1)^2$. The results presented in Table 1 indicate that the method proposed in this work converges with optimal rate to the solution of the problem and that the AFW based methods seem perform better than the PEERS for this example.

Table 1: Example 1, $\ell = 1$: PEERS$_\ell$–based discretization with $\ell = 1$. Number of degrees of freedom, meshsizes, Newton iteration, errors, and rates of convergence for the mixed approximations.

$\mathtt{DOF}$	h	$\mathtt{it}$	$\mathsf{e}(\mathbf{D})$	$\mathsf{r}(\mathbf{D})$	$\mathsf{e}(\boldsymbol{\sigma})$	$\mathsf{r}(\boldsymbol{\sigma})$	$\mathsf{e}(\mathbf{u})$	$\mathsf{r}(\mathbf{u})$	$\mathsf{e}(\boldsymbol{\gamma})$	$\mathsf{r}(\boldsymbol{\gamma})$	$\mathsf{e}(p)$	$\mathsf{r}(p)$
1778	0.354	12	1.80e-02	–	4.59e-02	–	4.59e-03	–	7.45e-03	–	1.84e-02	–
7010	0.177	10	5.36e-03	1.750	1.17e-02	1.970	1.15e-03	1.999	3.12e-03	1.257	4.51e-03	2.031
27842	0.088	8	1.48e-03	1.858	2.98e-03	1.977	2.87e-04	2.001	9.81e-04	1.668	1.12e-03	2.006
97562	0.047	6	4.42e-04	1.922	8.56e-04	1.983	8.15e-05	2.000	3.09e-04	1.840	3.19e-04	1.998
389522	0.024	4	1.14e-04	1.958	2.16e-04	1.990	2.04e-05	2.000	8.16e-05	1.919	8.00e-05	1.997
1081202	0.014	4	4.14e-05	1.977	7.78e-05	1.993	7.34e-06	2.000	3.00e-05	1.957	2.88e-05	1.998

Table 2: Example 1, $\ell = 1$: AFW$_\ell$–based discretization with $\ell = 1$. Number of degrees of freedom, meshsizes, Newton iteration, errors, and rates of convergence for the mixed approximations.

DOF	h	it	e($\mathbf{D}$)	r($\mathbf{D}$)	e($\boldsymbol{\sigma}$)	r($\boldsymbol{\sigma}$)	e($\mathbf{u}$)	r($\mathbf{u}$)	e($\boldsymbol{\gamma}$)	r($\boldsymbol{\gamma}$)	e(p)	r(p)
1393	0.354	10	2.21e-03	–	2.49e-02	–	4.57e-03	–	2.84e-03	–	1.73e-02	–
5473	0.177	7	5.35e-04	2.046	6.12e-03	2.027	1.15e-03	1.997	7.29e-04	1.963	4.33e-03	1.996
21697	0.088	5	1.32e-04	2.020	1.52e-03	2.013	2.87e-04	1.999	1.84e-04	1.983	1.08e-03	1.999
75961	0.047	4	3.73e-05	2.009	4.29e-04	2.008	8.15e-05	2.000	5.27e-05	1.992	3.08e-04	2.000
303121	0.024	3	9.29e-06	2.007	1.07e-04	2.008	2.04e-05	2.000	1.32e-05	1.997	7.70e-05	2.000
841201	0.014	3	3.34e-06	2.002	3.84e-05	2.002	7.34e-06	2.000	4.76e-06	1.998	2.77e-05	2.000

Example 2: Fluid Flow Through a Cavity 2D With Two Circular Obstacles

Motivated by [9, Section 2.1], we study the behavior of the regularized $\mu(I)$-rheology model of granular materials for fluid flow through a 2D cavity with two circular obstacles without manufactured solution. We consider the domain $\Omega = (0,1)^2 \setminus \Omega_c$, where

$$\Omega_c = \left\{(x_1, x_2) : \ (x_1 - 1/3)^2 + (x_2 - 1/3)^2 < 0.1^2\right\} \cup \left\{(x_1, x_2) : \ (x_1 - 2/3)^2 + (x_2 - 2/3)^2 < 0.1^2\right\},$$

with boundary Γ, whose part around the circles is given by $\Gamma_c = \partial\Omega_c$. The model parameters are chosen as $\mu_s = 0.36, \mu_d = 0.91, I_0 = 0.73, d = 0.05, \rho = 2500$, and the regularization factor is $\varepsilon = 1E-03$. Notice that the relation between the diameter of the particles d and the width of the cavity is $1:20$, whereas the radius of both circular obstacles is double that of d. The mean value of p is fixed as $\kappa = 100$, no presence of gravity is assumed, that is, $\mathbf{f} = \mathbf{0}$, and the boundaries conditions are

$$\mathbf{u} = (0.2\, x_2 - 0.1, 0)^{\mathrm{t}} \quad \text{on} \quad \Gamma \setminus \Gamma_c \quad \text{and} \quad \mathbf{u} = \mathbf{0} \quad \text{on} \quad \Gamma_c\,.$$

In particular, we impose that flows cannot go in nor out through Γ_c, whereas at the top and bottom of the domain flows are faster in opposite direction. In Figure 1, we display the computed internal friction coefficient, magnitude of the velocity and symmetric part of the velocity gradient, and pressure field, which were built using the mixed AFW$_0$-based scheme on a mesh with meshsize $h = 0.016$ and $18,423$ triangle elements (actually representing $332,573$ DOF). We observe higher velocities at the top and bottom of the boundary going to the right and left of the domain, respectively, as we expected, but also a circulation phenomenon on the left and right boundaries since the flows cannot in nor out through the circle obstacles. In addition, most of the variations in both the magnitude of the symmetric part of the velocity gradient tensor and pressure field occur around the circular obstacles. This observation aligns with the results obtained for the discrete internal friction coefficient. Notice also that between the circle obstacles and in some parts of the middle of the domain the magnitude of the symmetric part of the velocity gradient is zero or close to it and hence the granular flows are static. The latter is in agreement with the velocity of the fluid and it is overcome by the mixed approximation considering the regularized viscosity (5) as it was described in Section 2.

DOI: 10.5540/03.2025.011.01.0333

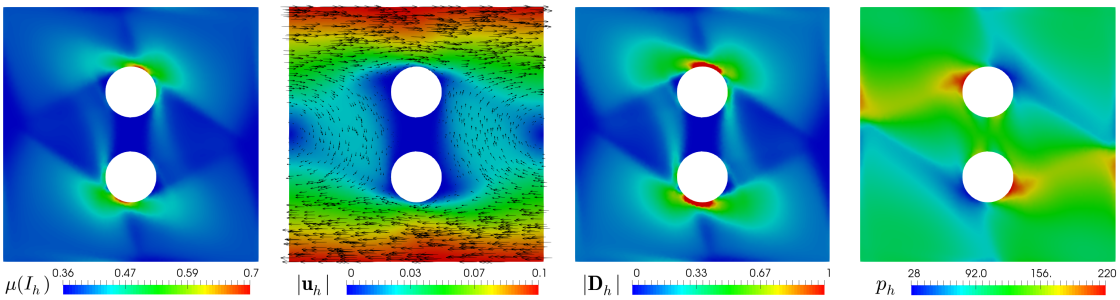

Figure 1: [Example 1] Computed internal friction coefficient, magnitude of the velocity and symmetric part of the velocity gradient, and pressure field. Figure by the authors

References

[1] M. Alnæs, J. Blechta, J. Hake, A. Johansson, B. Kehlet, A. Logg, C. Richardson, J. Ring, M. E. Rognes, and G. N. Wells. "The FEniCS project version 1.5". In: **Archive of numerical software** 3.100 (2015).

[2] D. Arnold, R. Falk, and R. Winther. "Mixed finite element methods for linear elasticity with weakly imposed symmetry". In: **Mathematics of Computation** 76.260 (2007), pp. 1699–1723.

[3] G. A. Benavides, S. Caucao, G. N. Gatica, and A. A. Hopper. "A Banach spaces-based analysis of a new mixed-primal finite element method for a coupled flow-transport problem". In: **Computer Methods in Applied Mechanics and Engineering** 371 (2020), p. 113285.

[4] S. Caucao, G. N. Gatica, S. R. Medrado, and Y. D. Sobral. "Nonlinear twofold saddle point-based mixed finite element methods for a regularized (I)-rheology model of granular materials". In: **Journal of Computational Physics** 520 (2025), p. 113462.

[5] S. Caucao, R. Oyarzúa, and S. Villa-Fuentes. "A new mixed-FEM for steady-state natural convection models allowing conservation of momentum and thermal energy." In: **Calcolo** 57.4 (2020).

[6] S. Caucao and I. Yotov. "A Banach space mixed formulation for the unsteady Brinkman–Forchheimer equations". In: **IMA Journal of Numerical Analysis** 41.4 (2021), pp. 2708–2743.

[7] E. Colmenares, G. N. Gatica, and J. C. Rojas. "A Banach spaces-based mixed-primal finite element method for the coupling of Brinkman flow and nonlinear transport". In: **Calcolo** 59.4 (2022), p. 51.

[8] L. Jing, C. Y. Kwok, Y. F. Leung, and Y. D. Sobral. "Characterization of base roughness for granular chute flows". In: **Physical Review E** 94.5 (2016), p. 052901.

[9] L. Jing, J. M. Ottino, P. B. Umbanhowar, and R. M. Lueptow. "Drag force in granular shear flows: regimes, scaling laws and implications for segregation". In: **Journal of Fluid Mechanics** 948 (2022), A24.

[10] P. Jop, Y. Forterre, and O. Pouliquen. "A constitutive law for dense granular flows". In: **Nature** 441.7094 (2006), pp. 727–730.

[11] S. B. Savage and K. Hutter. "The motion of a finite mass of granular material down a rough incline". In: **Journal of fluid mechanics** 199 (1989), pp. 177–215.

